RECONSTRUCTION FROM FLUORESCENCE CONFOCAL MICROSCOPY IMAGES

João Sanches Jorge S. Marques

Instituto Superior Técnico, Instituto de Sistemas e Robótica
Lisbon, Portugal

ABSTRACT

The fluorescence confocal microscopy is one of the most important tools in biomedical and pharmaceutic research. The main advantage of this technique over the traditional optical microscopy is the fact that it allows the selection of a thin cross-section of the sample by rejecting the visual information coming from the out of focus planes. Additionally, it uses fluorescence synthetic molecules that radiate in a wave length different from the one of the incident laser. It is easy to track these molecules inside the cell.

In this paper we present two related algorithms for fluorescence confocal microscopy, both of them derived from an alignment-by-reconstruction algorithm originally developed for 3D ultrasound. The first algorithm, estimates a 3D region from a set of images corresponding to a stack of parallel cross sections taken from the cell. The second algorithm, estimates one 2D cross-section from a set of images taken during a long period of time. This last algorithm also estimates a 2D function describing the intensity exponential decay fluorescence coefficients for each position on the 2D region of interest. This decrease of the image intensity, called photobleaching, must be compensated but it is useful from a biological point of view because it is related with the chemical and transport phenomena that occur inside the cell.

1. INTRODUCTION

Confocal microscopy is known since the end of fifties. However, the most significant advances occurred during the last decade. The fluorescence confocal microscope has became one of the most powerful tool in medical and biological research [4] due to the improvement of the laser scanning confocal microscope (LSCM) [3], to the development of synthetic fluorescent probes and proteins and to the development of a wider spectrum of laser light sources coupled to highly accurate acoustic/optic controlled filters.

The main advantage of the fluorescence confocal microscope over the traditional optical one consists on its capability of illuminate a thin plan of the specimen to be observed, collecting the light radiated from that plan and eliminating the out-of-focus information[2]. The illumination is provided by a highly focused laser beam and the observation is performed by rejecting all radiation but the one emitted by the fluorescence effect[1], as shown in Fig.1.

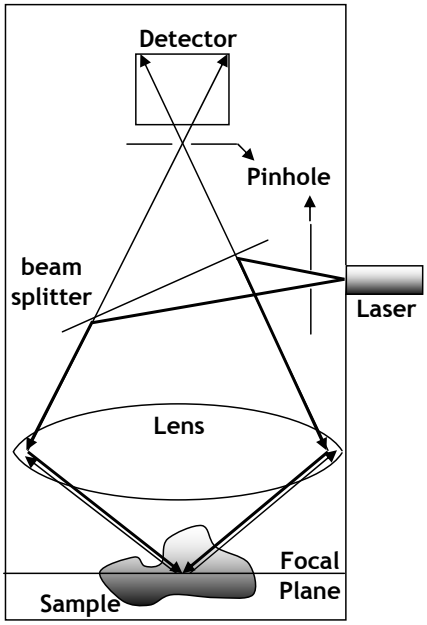

Fig. 1. Confocal Microscope.

By controlling the position of the sample or the geometry of the microscope (pinholes and lens positions) [3] it is possible to select the focal plane to be observed. This allows the extraction of a sequence of parallel cross-section of a specimen with small inter-planes contamination and reconstruct three dimensional structures, e.g., cytoplasmatic or nucleus membranes, cytoskeleton, mitochondria, Golgi apparatus, endoplasmic reticulum, and nucleus [6].

This paper presents a reconstruction algorithm from fluorescence confocal microscopy images, inspired in a 3D ultrasound reconstruction method presented in [5]. Here two different problems are considered, i) 3D reconstruction from a set of parallel cross-sections of the cell taken in a short period of time and ii) 2D reconstruction of a sin-

Corresponding author: J. Sanches (jmrs@alfa.ist.utl.pt)

gle plane from a set of images, corresponding to the same cross-section taken in a long period of time.

The four main difficulties that we must to deal with are the following:

1. Non Gaussian noise. Images are corrupted by multiplicative noise with a Poisson distribution. The noise arises because the number of emitted photons due the fluorescence effect is very small.

2. Unobserved inter-planes regions. When the vertical spatial resolution is small, some planar regions in between cross-sections, could not be observed. In these cases they must be estimated by interpolation.

3. Blurring. The rejection of visual information radiated from the out-of-focus planes is not perfect. Therefore, there is a blurring effect, described by a point spread function (PSF) [2] that can be included in the reconstruction algorithm. In this paper it will be assumed that this effect is negligible (future improvements will take it into account).

4. Photobleaching. This, phenomenon occurs when fluorophore permanently loses the ability to fluoresce, due to chemical reactions induced by the incident laser or by other surrounding molecules. This effect leads to a decrease in the image intensity along the time and at space varying rates. When the acquisition is fast and the laser intensity is low, as it is the case in data acquisition for 3D reconstruction, this phenomenon is not relevant. However, in long time acquisition processes this effect must be considered.

2. 3D RECONSTRUCTION

The 3D reconstruction of the cell from a set of parallel cross sections can be formulated as follows. Let f be a scalar function describing the fluorophore distribution in the region of interest (ROI) $\Omega \in \mathbb{R}^3$. We will assume that

$$f(\mathbf{x}) = \Phi(\mathbf{x})^T F \tag{1}$$

where $\Phi(\mathbf{x}) = [\phi_1(\mathbf{x}), \phi_2(\mathbf{x}), ..., \phi_N(\mathbf{x})]^T$ is a vector of N spline basis functions and $F = [f_1, f_2, ..., f_N]$ is a vector of coefficients to be estimated. We will assume that splines have a finite support and are centered at the nodes of a regular grid (see [11] for details). A typical grid has $100 \times 100 \times 100$ nodes.

The goal in this section is to estimate the function $f(\mathbf{x})$ from a set of noisy observations $Y = \{y^p_{i,j}\}$ and the corresponding locations, $X = \{\mathbf{x}^p_{i,j}\}$, affected by measurement errors, where $p = 0, ..., L-1$ and $0 \leq (i,j) \leq (n,m)$. The pixel locations in space in a cross-section p, is given by

$$\mathbf{x}^p_{i,j} = \mathbf{x}^p_0 + U_p \left[R_p[i,j]^T + T_p\right] \tag{2}$$

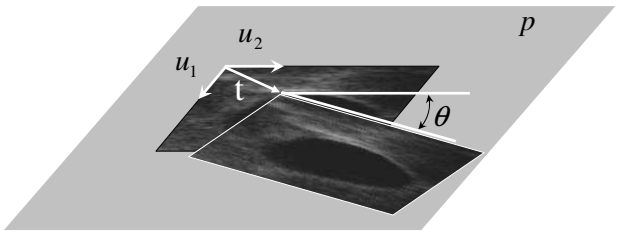

Fig. 2. Alignment by rotation and translation.

where $\mathbf{x}^p_0$ is the 3D location of the bottom-left pixel, $\mathbf{x}^p_{0,0}$, and $U_p = [\mathbf{u}^p_1, \mathbf{u}^p_2]$ is a 3×2 matrix (see Fig. 2). The two columns of U_p, $\mathbf{u}^p_1$ and $\mathbf{u}^p_2$, are the orthogonal vectors aligned with the image sides with length equal to the inter pixels distance. These parameters, $\mathbf{x}^p_0$, $\mathbf{u}^p_1$ and $\mathbf{u}^p_2$, are obtained from the position and orientation of each cross-section provided by the acquisition system and are affected by errors. To correct these errors, the pixel positions are rotated and translated by using a rotation matrix,

$$R_p = \begin{pmatrix} \cos(\theta) & -\sin(\theta) \\ \sin(\theta) & \cos(\theta) \end{pmatrix} \tag{3}$$

and the translation vector $\mathbf{t}_p = t^p_1 \mathbf{u}^p_1 + t^p_2 \mathbf{u}^p_2$. All these parameters, $\Psi = [(t_1, t_2, \theta)_p]$, with $p = 0, ..., L-1$, must be estimated during the reconstruction process.

The function $f(\mathbf{x})$ and pose parameters Ψ can be estimated by the maximum a posteriori (MAP) method. This leads to

$$[\hat{F}, \hat{\Psi}] = \arg\min_{F,\Psi} E(F, \Psi) \tag{4}$$

where

$$E(F, \Psi) = -\log(p(Y|F, \Psi)) - \log(p(F)) - \log(p(\Psi)) \tag{5}$$

is the energy function to be optimized.

1. In this expression $p(Y|F, \Psi)$ is the observation model which accounts for the multiplicative noise corrupting the confocal images. Assuming statistical independency of the observations [7] and a Poisson distribution for the pixel intensities [6], the data fidelity term is

$$E_Y = -\log(p(Y|F, \Psi)) = -\sum_{p=1}^{L} \sum_{i,j}^{n,m} \varphi(y^p_{i,j}, \mathbf{x}^p_{i,j}) \tag{6}$$

where $\mathbf{x}^p_{i,j}$ depends on $(t_1, t_2, \theta)_p$ and

$$\begin{aligned} \varphi(y, \mathbf{x}) &= \log\left[\frac{f(\mathbf{x})^y}{y!} e^{-f(\mathbf{x})}\right] \\ &= y \log[f(\mathbf{x})] - f(\mathbf{x}) + C. \end{aligned} \tag{7}$$

2. $p(F)$ is the prior associated to the vector of coefficients, F. The prior information allows us to deal with the ill-posed nature of the reconstruction problem [8].The prior $p(F)$ is assumed to be a Gibbs distribution with quadratic potential functions [9], i.e.,

$$p(F) = \frac{1}{Z} e^{-\gamma U(F)} \tag{8}$$

where γ is the regularization parameter and $U(F) = \sum_{(p,q)\in S} \delta_{pq}^2$ is the internal energy with $\delta_{pq}^2 = (f_p - f_q)^2$. This energy is obtained by summing all square differences among neighbouring nodes in the neighbor system S.

3. $p(\Psi)$ is the prior distribution of the alignment parameters, $(t_1, t_2, \theta)_p$. Assuming a zero mean normal distribution for the alignment parameters and statistical independency we obtain

$$p(\Psi) = C \prod_{p=0}^{L-1} e^{-\frac{(t_1^p)^2+(t_2^p)^2}{2\sigma_t^2} - \frac{(\theta^p)^2}{2\sigma_\theta^2}} \tag{9}$$

Using the previous models, the energy function (5) is

$$\begin{aligned} E(F,\Psi) &= -\sum_{p=1}^{L}\sum_{i,j}^{n,m} \varphi(y_{i,j}^p, \mathbf{x}_{i,j}^p) + \\ &\frac{1}{2\sigma_t^2}\sum_{p=1}^{L}\left[(t_1^p)^2 + (t_2^p)^2\right] + \frac{1}{2\sigma_\theta^2}\sum_{p=1}^{L}(\theta^p)^2 + \\ &\gamma \sum_{(p,q)\in S} (f_p - f_q)^2. \end{aligned} \tag{10}$$

where $f(x) = \sum_{k=0}^{N-1} f_k \phi_k(x)$ and $\mathbf{x}_{i,j}^p$ given by (2).

The minimization of (10) is an optimization problem with a very large number of variables. The solution of (4) can be obtained by finding the stationary point of $E(F,\Psi)$ w.r.t. F and Ψ, i.e., $\nabla_{F,\Psi} E(F,\Psi) = 0$. This is performed iteratively in two steps,

$$\nabla_F E(F, \hat{F}_{t-1}, \hat{\Psi}_{t-1}) = 0 \rightarrow \hat{F}_t \tag{11}$$

$$\nabla_\Psi E(\Psi, \hat{F}_t, \hat{\Psi}_{t-1}) = 0 \rightarrow \hat{\Psi}_t \tag{12}$$

where t denotes the tth iteration. These two steps alternates until convergence is achieved.

To solve the equations (11)-(12) we will use the Gauss-Seidel and fixed point methods by optimizing the energy function w.r.t. to each parameter, f_k, t_τ^p and θ_p at a time and keeping all the other unknowns constant [10].

From the stationary conditions, $\partial E(F,\Psi)/\partial f_k = 0$, $\partial E(F,\Psi)/\partial t_\tau^p = 0$ and $\partial E(F,\Psi)/\partial \theta_p = 0$ we obtain the following recursion expessions

$$\hat{f}_k^{t+1} = \frac{1}{2\gamma N_v}\sum_{p,i,j}^{L,n,m} \beta_{i,j}^p \phi_k(\hat{\mathbf{x}}_{i,j}^p) + \bar{f}_k^t \tag{13}$$

$$(t_\tau^p)^{t+1} = \sigma_t^2 \sum_{i,j}^{n,m} \beta_{i,j}^p \underbrace{(\nabla f(\hat{\mathbf{x}}_{i,j}^p).\mathbf{u}_\tau^p)}_{\text{dot product}} \tag{14}$$

$$(\theta_p)^{t+1} = \sigma_\theta^2 \sum_{i,j}^{n,m} \beta_{i,j}^p \underbrace{(\nabla f(\hat{\mathbf{x}}_{i,j}^p).\mathbf{v}_{i,j}^p)}_{\text{dot product}} \tag{15}$$

where

$$\begin{aligned} \beta_{i,j}^p &= \frac{y_{i,j}^p}{f(\mathbf{x}_{i,j}^p)} - 1 \\ \hat{\mathbf{x}}_{i,j}^p &= \mathbf{x}_0^p + (r_1^p(i,j) + t_1^p)\mathbf{u}_1^p + \\ &\quad (r_2^p(i,j) + t_2^p)\mathbf{u}_2^p \qquad (16) \\ \mathbf{v}_{i,j}^p &= -r_2^p(i,j)\mathbf{u}_1^p + r_1^p(i,j)\mathbf{u}_2^p \qquad (17) \\ r_1^p(i,j) &= i\cos(\theta_p) - j\sin(\theta_p) \qquad (18) \\ r_2^p(i,j) &= i\sin(\theta_p) + j\cos(\theta_p). \qquad (19) \end{aligned}$$

N_v is the number of neighbors of f_k and

$$\bar{f}_k^t = (1/N_v) \sum_{(p\in V_k)} \hat{f}_p^t \tag{20}$$

is the average intensity in the neighborhood of f_k. In the computation of the alignment parameters, $[t_1, t_2, \theta]^p$, only the pixels belonging to the pth cross-section are used.

The initialization of the unknowns is performed as follows,

$$f_k^0 = f_k^{ML} \qquad t_\tau^p = \theta = 0$$

where f_k^{ML} is an approximate maximum likelihood estimate given by

$$f_k^{ML} = \frac{\sum_{i\in V(f_k)} y_i \phi_k(x_i)}{\sum_{i\in V(f_k)} \phi_k(x_i)} \tag{21}$$

This expression is obtained assuming that $f(x_i) \approx f_k$ when x_i is in the neighborhood of f_k, $V(f_k)$.

3. 2D RECONSTRUCTION WITH PHOTOBLEACHING

The photobleaching occurs when a single plan is observed during a long period of time for studying the molecule transport and diffusion phenomena inside the cell[1]. In this case, the decreasing in the image intensity and cell movements must be compensated. Therefore, instead of estimating a 3D volume, as in the previous section, we want to estimate the underline 2D function that is being observed.

The formalization of the previous problem can still be used with the following modification: parameters of the Poisson distribution have an exponential decay along the time, i.e.,

$$f(x) \rightarrow f(x)e^{-\lambda(x)p} \tag{22}$$

where p is the index of the pth image and $\lambda(x)$ is a space varying coefficient characterizing the intensity decay. The function $\lambda(x)$ is now defined as linear combination of basis functions (compare with (1)),

$$\alpha(\mathbf{x}) = \Phi(\mathbf{x})^T \Lambda \tag{23}$$

where $\Lambda = [\lambda_1, \lambda_2, ..., \lambda_N]$ is to be estimated. Additionally, the vectors U_p are the same for all planes, that is, $U^p = U = [\mathbf{u}_1, \mathbf{u}_2]$.

The equation (7) is now replaced by

$$\varphi(y, \mathbf{x}) = y \log(f(\mathbf{x})) - \lambda(\mathbf{x})yp - f(\mathbf{x})e^{-\lambda(\mathbf{x})p} \tag{24}$$

and the new energy function is

$$\begin{aligned} E(F, \Lambda, \Psi) \quad = \quad & -\sum_{p=1}^{L}\sum_{i,j}^{n,m} \varphi(y_{i,j}^p, \mathbf{x}_{i,j}^p) + \\ & \frac{1}{2\sigma_t^2}\sum_{p=1}^{L}\left[(t_1^p)^2 + (t_2^p)^2\right] + \frac{1}{2\sigma_\theta^2}\sum_{p=1}^{L}(\theta^p)^2 + \\ & \gamma \sum_{(p,q)\in S}(f_p - f_q)^2 + \\ & \rho \sum_{(p,q)\in S}(\lambda_p - \lambda_q)^2 \end{aligned} \tag{25}$$

where ρ is a regularization parameter for the $\lambda(x)$ field. The recursion equations are derived in the same way as previously, leading to

$$\hat{f}_k^{t+1} = \frac{1}{2\gamma N_v}\sum_{p,i,j}^{L,n,m} \beta_{i,j}^p \phi_k(\hat{\mathbf{x}}_{i,j}^p) + \bar{f}_k^t \tag{26}$$

$$\hat{\lambda}_k^{t+1} = \frac{1}{2\gamma N_v}\sum_{p,i,j}^{L,n,m} \omega_{i,j}^p \phi_k(\hat{\mathbf{x}}_{i,j}^p) + \bar{\lambda}_k^t \tag{27}$$

$$(t_\tau^p)^{t+1} = \sigma_t^2 \sum_{i,j}^{n,m} \underbrace{\mathbf{d}_{i,j}^p . \mathbf{u}_\tau^p}_{\text{dot product}} \tag{28}$$

$$(\theta_p)^{t+1} = \sigma_\theta^2 \sum_{i,j}^{n,m} \underbrace{\mathbf{d}_{i,j}^p . \mathbf{v}_{i,j}^p}_{\text{dot product}} \tag{29}$$

where

$$\begin{aligned} \beta_{i,j}^p &= \frac{y_{i,j}^p}{f(\mathbf{x}_{i,j}^p)} - e^{-\lambda(\mathbf{x}_{i,j}^p)p} \\ \omega_{i,j}^p &= p\left[f(\mathbf{x}_{i,j}^p)e^{-\lambda(\mathbf{x}_{i,j}^p)p} - y_{i,j}^p\right] \\ \mathbf{d}_{i,j}^p &= \beta_{i,j}^p \nabla \mathbf{f}(\hat{\mathbf{x}}_{i,j}^p) + \omega_{i,j}^p \nabla\lambda(\hat{\mathbf{x}}_{i,j}^p). \end{aligned} \tag{30}$$

The auxiliary unknowns $\hat{\mathbf{x}}_{i,j}^p$, $\mathbf{v}_{i,j}^p$, $r_1^p(i,j)$ and $r_2^p(i,j)$ are defined by equations (16)-(19). The coefficients λ_k are initalized with zeros, i.e., $\lambda_k^0 = 0$.

The equations (26)-(29) are alternatively computed until convergence is achieved. The field $\lambda(x)$ contains useful biological information, because it provides the decreasing rate of the fluorophore at different locations of the cell, which is related with the chemical and diffusion processes involved.

4. EXPERIMENTAL RESULTS

In this section two examples using real data are presented. In the first example a set of 20 images are used for the 3D reconstruction of the cell. These images, correspond to parallel cross sections of a cell taken in a short period of time to avoid the photobleaching effect. Figs. 3 a-c) show three images from the data sequence used by the reconstruction algorithm. Figs. 3 d-f) show three different views of the 3D reconstruction of the cell cytoplasmatic membrane.

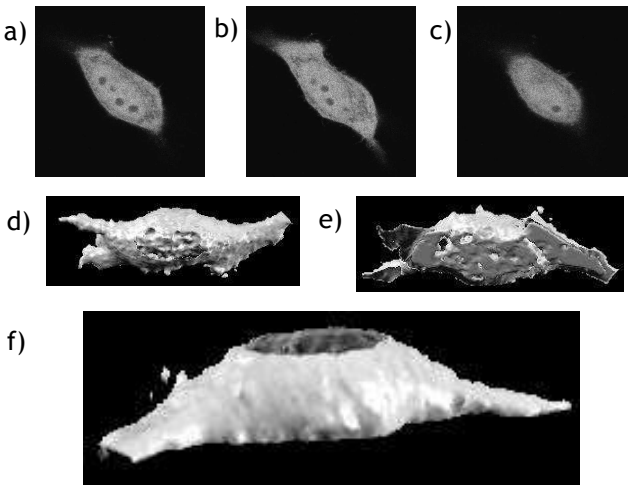

Fig. 3. 3D reconstruction from 20 images. a-c)Three noisy images from the data sequence used for 3D reconstruction. d-f) Three different views of the 3D reconstructed cytoplamatic membrane.

The second example results are displayed in Fig. 4 and corresponds to the 2D reconstruction of a single cross-section of a cell from a set of 300 images with photobleaching. Figs. 4a-b) display the first and the 100th images of the data sequence, respectively, where the photobleaching effect is clear, since the second image is much more less intense than the first one. Figs. 4 c-d) display the estimated function $f(\mathbf{x})$ and the corresponding function of intensity exponential decay coefficients, $\lambda(\mathbf{x})$, respectively.

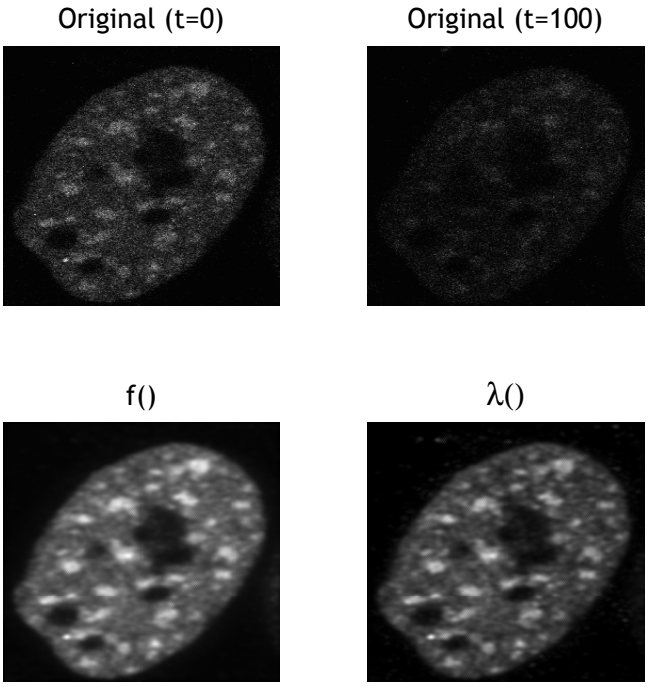

Fig. 4. 2D reconstruction with photobleaching. First line: First and 100th image respectively from a sequence of 300 images. Second line: Estimated 2D functions $f(x)$ and $\lambda(x)$ respectively.

5. CONCLUSIONS

In this paper we present two algorithms for fluorescence confocal microscopy, based on the alignment-by-reconstruction algorithm developed for 3D ultrasound. The first algorithm estimates a 3D region of interest from a set of fluorescence confocal images corresponding to parallel cross-sections uniformly taken from the volume. These images are corrupted by Poisson noise and are misaligned. The reconstruction algorithm deals with these difficulties by reducing the noise and estimating the geometric transformation needed to perform the alignment. This is done in a unified way, by minimizing the same energy function w.r.t. both sets of parameters: 3D function and alignment coefficients.

The second algorithm estimates a 2D function from a set of fluorescence confocal images corresponding to the same cross-section. These images are obtained during a long period o time. Therefore, a decreasing of intensity, called photobleaching, is observed and must be compensated. Additionally, during this long period of time, the cell moves and its displacement must be compensated, as in the previous 3D reconstruction algorithm. The photobleaching is compensated by estimating a 2D function, corresponding to the exponential decreasing rate at each pixel. The 2D function, exponential coefficients and alignment parameters are estimated simultaneously.

6. REFERENCES

[1] Kevin Braeckmans, Fotobleaching with the confocal laser scanning micrscope for mobility measurments and the encoding of microbeads, PhD Thesis, University of Gent, 2004.

[2] Nabil Aly Mohamed Aly Lashin, Restoration Methods For Biomedical Images In Confocal Microscopy, PhD. Thesis, Berlin 2005.

[3] Handbook of Biological Confocal Miscroscopy. New York: Plenum Press, 1995.

[4] Molecular Expressions. Optical Micrscopy Primer, http://micro.magnet.fsu.edu/primer/index.html

[5] João Sanches, Jorge S. Marques, Joint Image Registration and Volume Reconstruction for 3D Ultrasound, Special Issue on 3D Ultrasound, Pattern Recognition Letters 24(2003) 791-800.

[6] Peter J. Verveer. Computational and optical methods for improving resolution and signal quallity in fuorescence microscopy. PhD thesis, Department of imaging science and technology, faculty of applied sciences, Delft university of technology, 1998.

[7] E. Rignot, R. Chelappa, Segmentation of polarimetric sunthetic aperture radar data, IEEE Trans. Image Processing, vol.1, no.1, pp. 281-300, 1992.

[8] C.R. Vogel, Computational Methods for Inverse Problems, Frontiers in applied mathematics - SIAM, 2002.

[9] S. Geman and D. Geman, Stochastic Relaxation, Gibbs Distributions, and the Bayesian Restoration of Images, IEEE Trans on Pattern Analysis and Machine Intelligence, vol.PAMI-6, no.6, pp.721-741, November 1984.

[10] W.H.Press, W.T.Vetterling, S.A.Teukolsky and B.P.Flanner, Numerical Recipes in C, Cambridge University Press, 1994

[11] João Sanches, Jorge S. Marques, A Rayleigh reconstruction/interpolation algorithm for 3D ultrasound, Pattern Recognition Letters, 21, pp. 917-926, 2000.